Evolution Behavior of Precipitated Phases During Aging Treatment of Al-Cu3-Si-Mg Alloy by MMDF

Tong Wu and Shuming Xing *

Posted Date: 21 April 2026

doi: 10.20944/preprints202604.1453.v1

Keywords: molten metal die forging; Al-Cu3-Si-Mg alloy; aging treatment; precipitated phases; evolution behavior

 doi:10.20944/preprints202604.1453.v1

Article

Evolution Behavior of Precipitated Phases During Aging Treatment of Al-Cu3-Si-Mg Alloy by MMDF

Tong Wu and Shuming Xing *

School of Mechanical and Electronic Control Engineering, Beijing Jiaotong University, Beijing 100044, China

* Correspondence: smxing@bjtu.edu.cn; Tel.: +86-136-4115-6691

Abstract

In this paper, the supersaturated solid solution of Al-Cu3-Si-Mg alloy prepared by molten metal die forging (MMDF) was used as the research object. The formation and evolution of precipitates during aging treatment were investigated through experiments at different temperatures and times, and the precipitation mechanisms and sequences of various precipitates were analyzed. The main precipitated phases formed in the supersaturated solid solution of Al-Cu3-Si-Mg alloy after aging treatment are θ(Al_2Cu), θ'($Al_{3.6}Cu_2$), γ'($Al_{0.63}Mg_{0.37}$) and η'(Cu, Si). Based on XRD and TEM analysis under different aging treatment conditions, the precipitation sequence is determined as follows: SSS → GP_0 → GP_0+γ'→GP_0+(γ'+γ)+θ''+η'→(γ'+γ)+(θ''+θ')+(η'+η)→(γ'+γ)+(θ+θ')+(η'+η)→(γ'+γ)+(θ+θ')+η→γ+θ+η. With increasing aging temperature and time, precipitates tend to accumulate at the α-Al grain boundaries. After aging treatment at 165-185 °C for 4 h, chain-like θ(Al_2Cu) precipitates are discontinuously distributed at the α-Al grain boundaries, disk-shaped θ'($Al_{3.6}Cu_2$) and θ''(Al_2Cu) phases mainly precipitate within the grains. When the temperature exceeds 185 °C, the chain-like θ(Al_2Cu) precipitates at the grain boundaries gradually become continuous, the amount of θ(Al_2Cu) phase in the grains increases significantly, θ''(Al_2Cu) disappears completely, and the size of θ'($Al_{3.6}Cu_2$) decreases obviously. After aging treatment at 185 °C for 5-6 h, the chain-like θ(Al_2Cu) precipitates at the grain boundaries become more continuous, and their length fraction f_L^θ continues to increase with prolonged aging time.

Keywords: molten metal die forging; Al-Cu3-Si-Mg alloy; aging treatment; precipitated phases; evolution behavior

1. Introduction

As a wrought aluminum alloy, the Al-Cu3-Si-Mg alloy exhibits poor castability, castings produced by conventional casting techniques contain numerous defects, and their properties cannot meet the requirements. Using the Molten metal die forging (MMDF) process to prepare wrought aluminum alloy castings allows pressure to be applied during the solidification of the molten metal, featuring characteristics of both casting and forging. The applied pressure exerts a rheological feeding effect, which overcomes the casting difficulties of high-strength wrought aluminum alloys caused by poor fluidity, while achieving better mechanical properties than conventional cast aluminum alloys [1–3]. Compared with gravity casting, the wrought aluminum alloy fabricated under pressure via MMDF exhibits refined microstructure and increased solid solubility of strengthening elements such as Cu. This indicates that pressure can suppress the solute diffusion coefficient at the solid-liquid interface and enhance the solute solubility in the matrix. The dissolution of these second phases facilitates the subsequent heat treatment strengthening process [4–8].

Precipitation hardening is the primary strengthening mechanism during aging treatment of Al-Cu alloys, which can significantly improve the overall strength of the alloy. By optimizing the aging temperature and time, finely dispersed and uniformly distributed strengthening precipitates can be obtained [9]. The morphology, size and distribution of these strengthening phases directly affect the mechanical properties of the material. Investigating the microstructural evolution during the aging

 doi:10.20944/preprints202604.1453.v1

process of Al–Cu alloys is of great significance for further optimizing the alloy properties [10]. Gazizov et al. [11] investigated the aging treatment at 170 °C on Al-4.9Cu alloy. With the progress of aging, the number of precipitates in the matrix gradually increased, and their morphology changed from disk-like/needle-rod shape to spherical shape. SAED analysis revealed that the transformation sequence of precipitates was GP → θ'' → θ'. Kim et al. [12] calculated the morphology factor of the θ' precipitate using first-principles calculations and found that the aspect ratio of the equilibrium precipitate decreases with increasing precipitate size. Tohid et al. [13] proposed a mixed model for isothermal heat treatment and combined with DSC measurements, simulated the growth kinetic pathways and sequences of precipitates in Al-Cu alloys, obtaining variation curves of precipitate type and size at different aging temperatures.

Dispersed strengthening precipitates significantly affect the mechanical properties of the alloy. Investigating the formation mechanism and sequence of precipitates in Al-Cu alloys prepared by MMDF after aging treatment is of great guiding significance for engineering applications. In this paper, the supersaturated solid solution in the as-cast microstructure of Al-Cu3-Si-Mg alloy prepared by MMDF was subjected to aging treatment at various temperatures and times. The precipitation mechanism and sequence of strengthening phases during aging treatment were explored, and the precipitation behavior of strengthening phases under different aging conditions was investigated.

2. Materials and Methods

2.1. Experimental Materials and Preparation Methods

The raw material used in this experiment is high-strength wrought aluminum-copper alloy 2A50 (China Brand), the alloy composition is shown in Table 1. Within the standard range, the Cu content is increased to the upper limit of 2.3-2.6% to improve the strength, hardness and machinability of the alloy. Properly reduce the Si content to 0.7% to prevent the formation of brittle silicides in the solidified microstructure. On this basis, appropriate amounts of rare earth elements La/Ce and Ti are added to achieve the effects of purification and grain refinement.

Table 1. Composition of 2A50 alloy (China Brand).

Grade	Composition (wt%)								
	Cu	**Si**	**Mg**	**Mn**	**Ti**	**Ni**	**Zn**	**Fe**	**Al**
2A50	1.8-2.6	0.5-0.7	0.7-0.8	0.42-0.57	0.05-0.01	0.001-0.009	0.012-0.020	0.07-0.20	Bal

The alloy melting procedure is shown in Figure 1. The 2A50 alloy was melted in the smelting furnace (YN-R-500-1200T, Shin Hing Technology Co. Ltd., Zhengzhou, China) at a temperature of 760 °C. After complete melting, the molten alloy was poured into the transfer ladle, and 2% rod-shaped rare earth master alloy Al-10La/Ce with a diameter of 10 mm and a length of 50 mm was added for modification treatment. 0.1% Al5Ti1B grain refiner was pressed into the molten metal using a bell jar, and argon gas was introduced for degassing for 12 minutes. After thorough stirring, the slag was skimmed off. The refined molten metal was poured into the automatic pouring device (W650 SVPC, Chensong Shape Machinery Co. Ltd., Cangzhou, China) for casting preparation.

 doi:10.20944/preprints202604.1453.v1

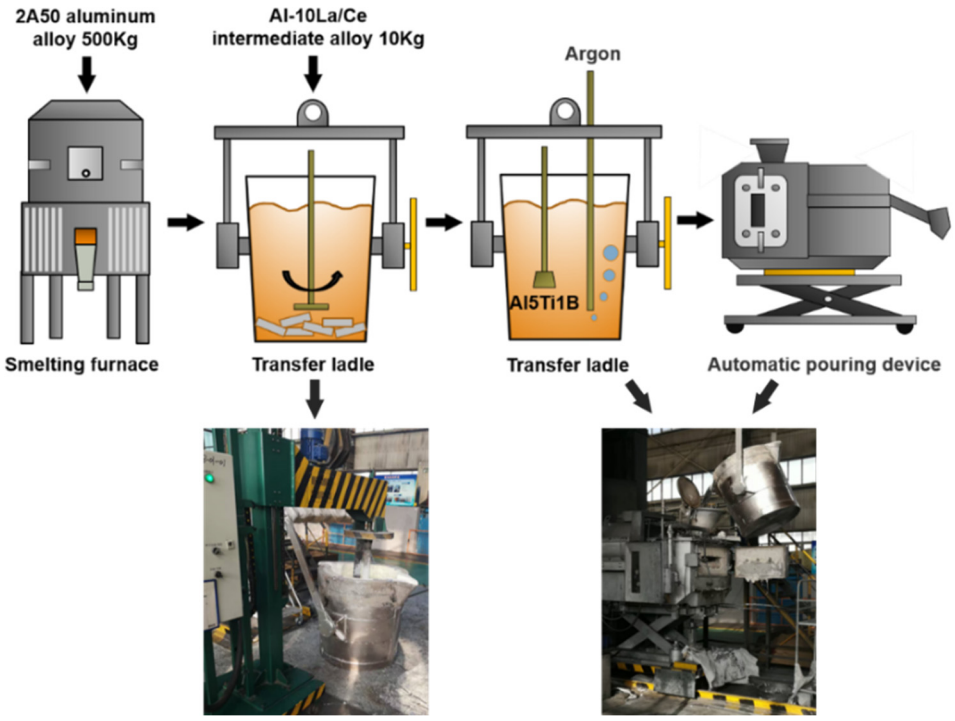

Figure 1. Schematic diagram of the melting process of Al-Cu3-Si-Mg alloy.

Prior to pouring the molten metal, components that come into direct contact with the molten metal, such as launders, were preheated to 700 ℃. Sample was taken before pouring for spectral element analysis, and the alloy composition obtained is shown in Table 2.

Table 2. Composition of the Al-Cu3-Si-Mg alloy.

Sample	Composition (wt%)								
	Cu	Si	Mg	Mn	Ti	Fe	La/Ce	Zn	Al
1	2.39	0.69	0.8	0.48	0.07	0.009	0.15	0.18	Bal

2.2. Experimental Equipment and Process

The wheel-shaped parts were fabricated by MMDF at a pressure of 118 MPa. MMDF was carried out using a 3000-ton vertical MMDF machine (THP16-3000, Tianduan Press Machine Co. Ltd., Tianjin, China). The upper and lower molds of the wheel-shaped part mold were respectively installed on the movable crossbeam and the working table of the MMDF machine. The mold structure and preparation process are shown in Figure 2a-d. The material of the mold is H13 steel, and is subjected to vacuum heat treatment. The bottom samples of the wheel-shaped parts were subjected to heat treatment, and the sampling positions are shown in Figure 2e.

 doi:10.20944/preprints202604.1453.v1

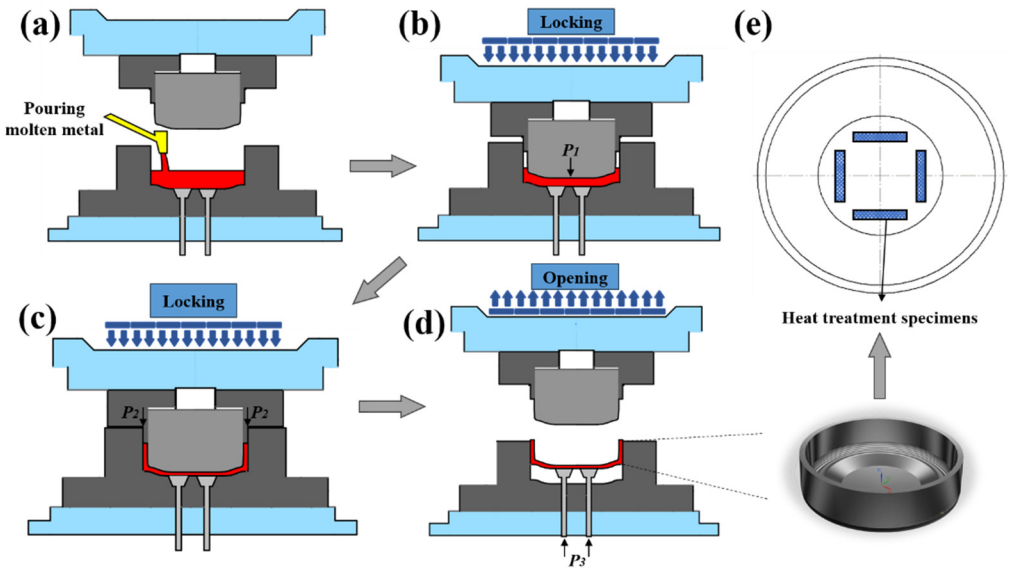

Figure 2. MMDF pressing process: (a) pouring; (b) internal ram compression; (c) external ram feeding; (d) die opening and part ejection; (e) sampling location.

2.3. Heat Treatment Experiments

The Al-Cu3-Si-Mg alloy specimens were cut into 10×10×10 mm^3 cubic samples for heat treatment. The samples were placed at the center of the heat treatment furnace (BFX-12C, Fulaimeng Experimental Equipment Co. Ltd., Beijing, China), heated from room temperature to 510 ℃ for 10 minutes, held at temperature for 60 minutes, then quenched in water at 25 ℃. Previous study shown that, under this solution treatment conditions, the coarse phases such as the eutectic E (Al_2Cu) and the secondary phase θ (Al_2Cu) in the supersaturated solid solution are fully dissolved into the α-Al matrix, facilitating the observation of the evolution of precipitated phases during aging treatment [14]. The solution-treated specimens were subjected to aging treatment experiment, the aging treatment scheme is shown in Table 3.

Table 3. Aging treatment experiment scheme.

Sample No.	Aging treatment parameters		
	Temperature (℃)	time (h)	Cooling method
1	165	4	Air cooling
2	175	4	Air cooling
3	185	2	Air cooling
4	185	3	Air cooling
5	185	4	Air cooling
6	185	5	Air cooling
7	185	6	Air cooling
8	195	4	Air cooling
9	205	4	Air cooling

The solution-treated specimens were placed at the center of the heat treatment furnace, heated from room temperature to 165 °C, 175 °C, 185 °C, 195 °C and 205 °C with a heating duration of 10 min. After held at temperature for 2 h, 3 h, 4 h, 5 h and 6 h respectively, the specimens were taken out and cooled in air. The heat treatment process curve is shown in Figure 3.

 doi:10.20944/preprints202604.1453.v1

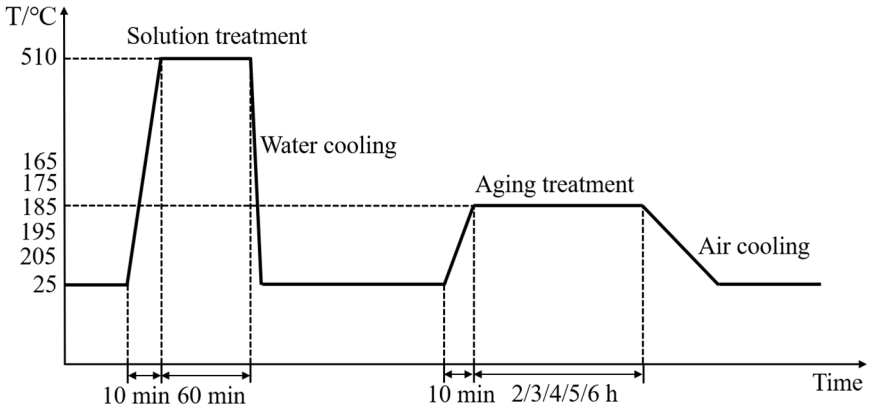

Figure 3. Heat treatment process curve.

2.4. Analysis Instruments

The microstructure of the Al-Cu3-Si-Mg alloy after aging treatment was observed by optical microscopy (OM, DM2000, Leica Microsystems, Wetzlar, Germany) and transmission electron microscope (TEM, FEI Talos F200X, Thermo Fisher Scientific, Eindhoven, Netherlands). The specimens for OM were ground by silicon carbide sandpaper. After the sample surface was smoothed, it was polished with 0.3 μm Al_2O_3 suspension until a mirror-like surface was obtained. The polished specimens were etched by Keller's reagent (95 mL H_2O + 2.5 mL HNO_3 + 1.5 mL HCl + 1.0 mL HF) for 15 seconds. TEM specimens were prepared by cutting 1 mm thick slices from the heat treatment samples. The slices were ground to less than 50 μm with sandpaper and then thinned by ion milling system (EM RES102, Leica Microsystems, Wetzlar, Germany). Phase analysis of the heat treatment specimens was performed by an X-ray diffractometer (D8 Advance, Bruker AXS GmbH, Karlsruhe, Germany) with a Cu target radiation source. The Kα wavelength was 0.15406 nm, the operating voltage was 40 kV, and the current was 40 mA. The scanning speed was set at 5 °/min, the scanning angle ranged from 10° to 90°, with a step size of 0.02 °, and the total test duration was 16 min.

3. Results

3.1. Formation Mechanism of Precipitated Phases During Aging Treatment

XRD analysis was performed on Al-Cu3-Si-Mg alloy specimens under different aging treatment conditions, as shown in Figure 4. It can be found that after aging treatment at 165 °C×2 h and 205 °C×6 h, the XRD patterns show that the main diffraction peaks correspond to α-Al, indicating that the matrix of the alloy after aging treatment is still composed of primary α-Al phase. The main weak diffraction peaks correspond to θ(Al_2Cu), θ' ($Al_{3.6}Cu_2$), $Al_{0.63}Mg_{0.37}$ and (Cu, Si). Among them, θ(Al_2Cu) exhibits a complex tetragonal crystal structure with lattice parameters $a=b$=6.064 Å, c=4.874 Å; θ'($Al_{3.6}Cu_2$) possesses a different structure from θ(Al_2Cu), presenting a simple tetragonal crystal structure with lattice parameters $a=b$=4.04 Å; $Al_{0.63}Mg_{0.37}$ phase exhibits a face-centered cubic crystal structure with lattice parameters $a=b=c$=4.216 Å and is designated as γ'; (Cu, Si) phase has lattice parameters $a=b$=7.267 Å, c=7.892 Å and is designated as η′.

XRD analysis also reveals that the intensities of the phase diffraction peaks vary under different aging treatment conditions, indicating that the amounts of the phases may change with different aging treatments. Figure 5 shows the enlarged XRD patterns of each phase at the same diffraction angle. It can be observed that when the aging treatment is changed from 165 °C×2 h to 205 °C×6 h, the peak areas of both θ(Al_2Cu) and η'(Cu, Si) tend to increase, while θ′($Al_{3.6}Cu_2$) decreases slightly. Indicating that with more sufficient aging treatment, the amounts of θ(Al_2Cu) and η'(Cu, Si) increase significantly. This may be attributed to their direct precipitation from the matrix or transformation from other transitional phases. The decrease in the amount of θ′($Al_{3.6}Cu_2$) may result from its

 doi:10.20944/preprints202604.1453.v1

transformation into other phases. The peak area of the γ'($Al_{0.63}Mg_{0.37}$) phase decreases slightly, indicating that it precipitates continuously under both aging conditions and transforms into other phases simultaneously.

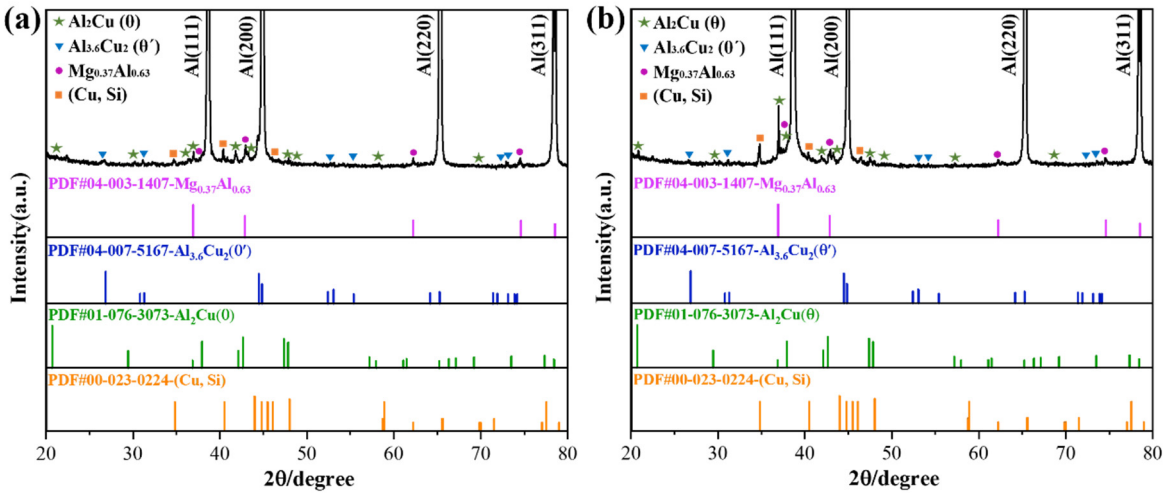

Figure 4. XRD analysis of Al-Cu3-Si-Mg alloy after aging treatment: (a) 165 °C×2 h; (b) 205 °C×6 h.

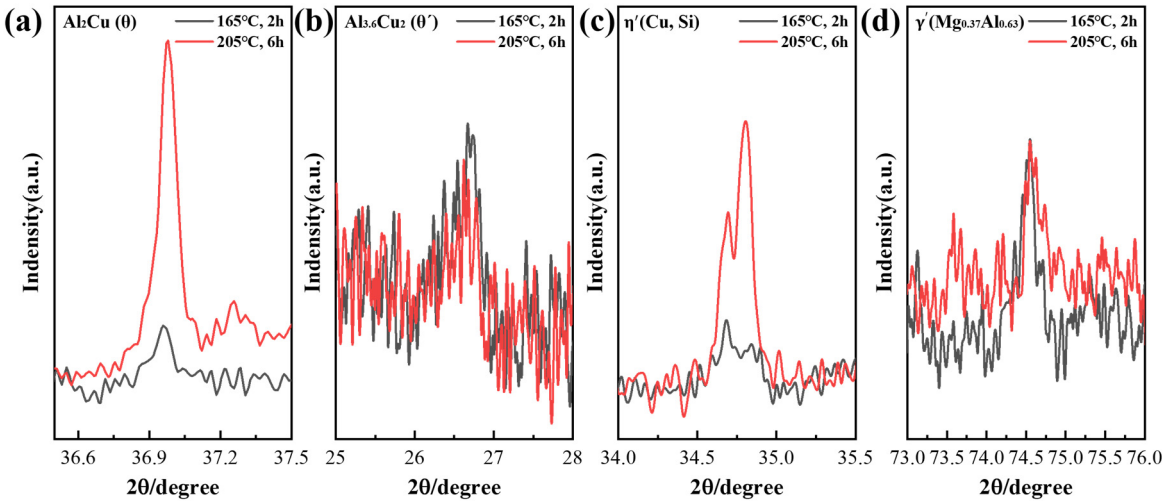

Figure 5. Local enlarged XRD patterns of the aging treatment structure of the Al-Cu3-Si-Mg alloy: (a) θ(Al_2Cu); (b) θ′($Al_{3.6}Cu_2$); (c) η′(Cu, Si); (d) γ′($Al_{0.63}Mg_{0.37}$).

Previous study has shown that after solution treatment, the eutectic phases E(Al_2Cu), β(Mg_2Si), Q($Al_5Cu_2Mg_8Si_6$) and the secondary phase θ(Al_2Cu) in the microstructure of the Al-Cu3-Si-Mg alloy dissolve into the α-Al matrix, forming a thermodynamically unstable solid solution with Cu, Mg and Si as the main solute elements [14]. During aging treatment, low-temperature heating allows these solute atoms to diffuse and cluster gradually, resulting in the precipitation of fine, uniformly dispersed strengthening phases. The microstructure of the sample aging at 165 °C×2 h is presented in Figure 6. It can be seen that the matrix of the supersaturated solid solution in the Al-Cu3-Si-Mg alloy is equiaxed α-Al phase. Different α-Al grains exhibit contrast variations under observation, which is caused by the differences in the distribution of secondary phases or the extent of lattice distortion in the matrix during aging treatment. The nanoscale secondary phase particles formed by the segregation of Cu, Mg, and Si elements after aging differ from the α-Al matrix in crystal structure and atomic arrangement, thus showing different reflectivity under optical microscopy. Accordingly, the bright regions contain a relatively low content of precipitates, while the dark regions are characterized by a dense distribution of precipitates. Figure 6b shows that chain-like precipitates are

 doi:10.20944/preprints202604.1453.v1

aggregated and distributed at some triangular grain boundaries of α-Al. Chain-like and discontinuously distributed precipitates can also be observed at the interfaces between some α-Al grains and rare-earth phases in Figures 6c, e. All of them consist of $\theta(Al_2Cu)$ formed by the segregation of Cu atoms at grain boundaries. It can be seen from Figure 6d that fine particles are dispersedly distributed within the α-Al grains.

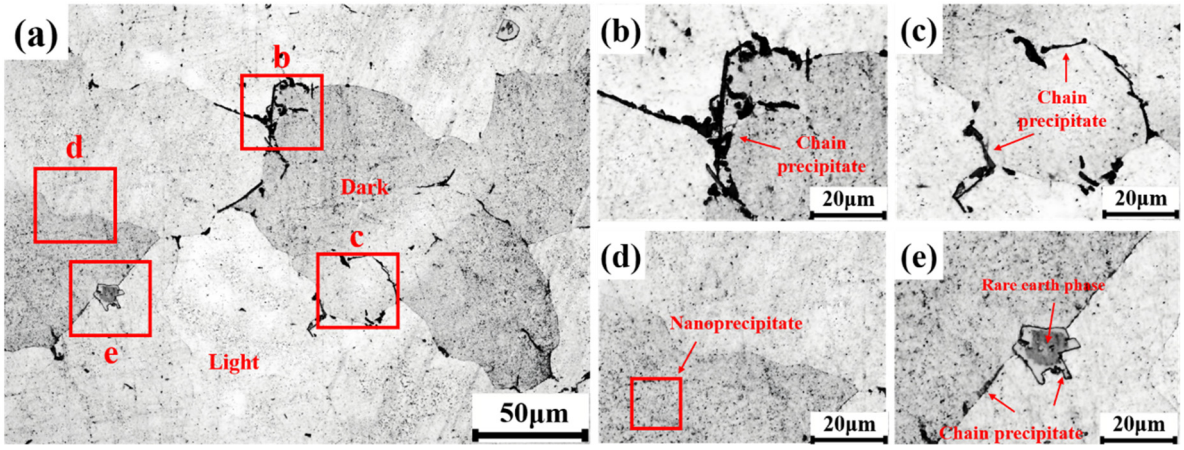

Figure 6. Microstructure of Al-Cu3-Si-Mg alloy after aging treatment (165 °C×2 h), OM: (a) low-magnification image; (b) α-Al triangular grain boundaries; (c) α-Al grain boundary; (d) α-Al intragranular precipitates; (e) rare earth phase.

The microstructure of the alloy aging at 205 °C×6 h is shown in Figure 7. It can be observed that the number of dark α-Al grains in the matrix increases, indicating an increase in precipitates under this condition. Figure 7b reveals that the chain-like precipitates aggregated at the triangular grain boundaries of α-Al transform into a network-like structure. This is attributed to the excessive aging temperature or prolonged holding time, which cause the $\theta(Al_2Cu)$ phases to increase and coarsen, resulting in the aggregation of chain-like precipitates into a network. Figures 7c-e show that the amounts of chain-like precipitates at the interfaces between α-Al grains and rare-earth phases, as well as the dispersive intragranular precipitates within α-Al grains, are both significantly increased.

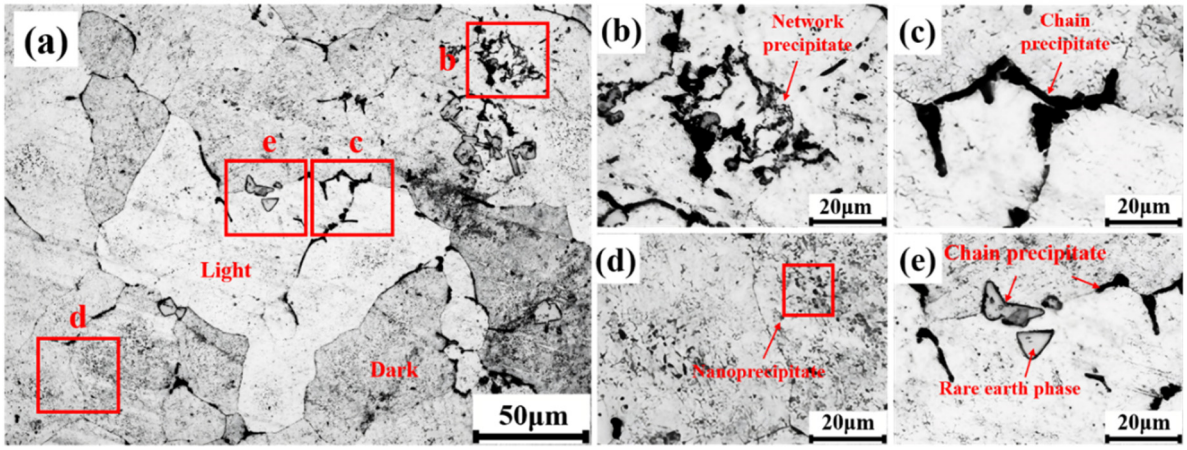

Figure 7. Microstructure of Al-Cu3-Si-Mg alloy after aging treatment (205 °C×6 h), OM: (a) low-magnification image; (b) α-Al triangular grain boundaries; (c) α-Al grain boundary; (d) α-Al intragranular precipitates; (e) rare earth phase.

TEM images of precipitates after aging treatment are shown in Figure 8. It can be seen from Figure 8a that disk-shaped $\theta'(Al_{3.6}Cu_2)$ precipitates with a size of approximately 60-70 nm are formed

 doi:10.20944/preprints202604.1453.v1

within the α-Al grains under aging treatment at 165 °C×2 h. Finer Cu atom-enriched GP zones and lamellar transitional θ''(Al_2Cu) phases are also present. Figure 8a_1 reveals that the GP zones are disc-shaped with a diameter of about 5-6 nm, showing no distinct interface with the matrix. SAED exhibits diffraction spots of the α-Al matrix along the [001] orientation, with no independent satellite spots or obvious diffraction streaks from the GP zones, indicating that the GP zones under this condition are close to the stage of transforming into θ''(Al_2Cu).Figures 8b, c show that γ'($Al_{0.63}Mg_{0.37}$) phases and η'(Cu, Si) phases exist within α-Al grains under both aging treatment. As shown in Figure 8b_1, γ'($Al_{0.63}Mg_{0.37}$) appears as aggregates of spherical particles with a diameter of 10-15 nm. Similar to GP zones, SAED only shows diffraction spots of the α-Al matrix along the [$\bar{1}$00] orientation, confirming it as an Mg atom-enriched region. For η'(Cu, Si), previous study has reported its chemical formula as $Cu_{3+x}Si$, which is also a transitional phase that exists as the equilibrium η(Cu_3Si) phase under stable conditions [15]. Figure 8d shows that relatively coarse θ(Al_2Cu) phases with a size of about 500 nm are present at α-Al grain boundaries after aging at 205 °C×6 h. SAED patterns exhibit additional quadrilateral spots superimposed on the matrix spots, with larger spot spacing compared with those of θ'($Al_{3.6}Cu_2$).

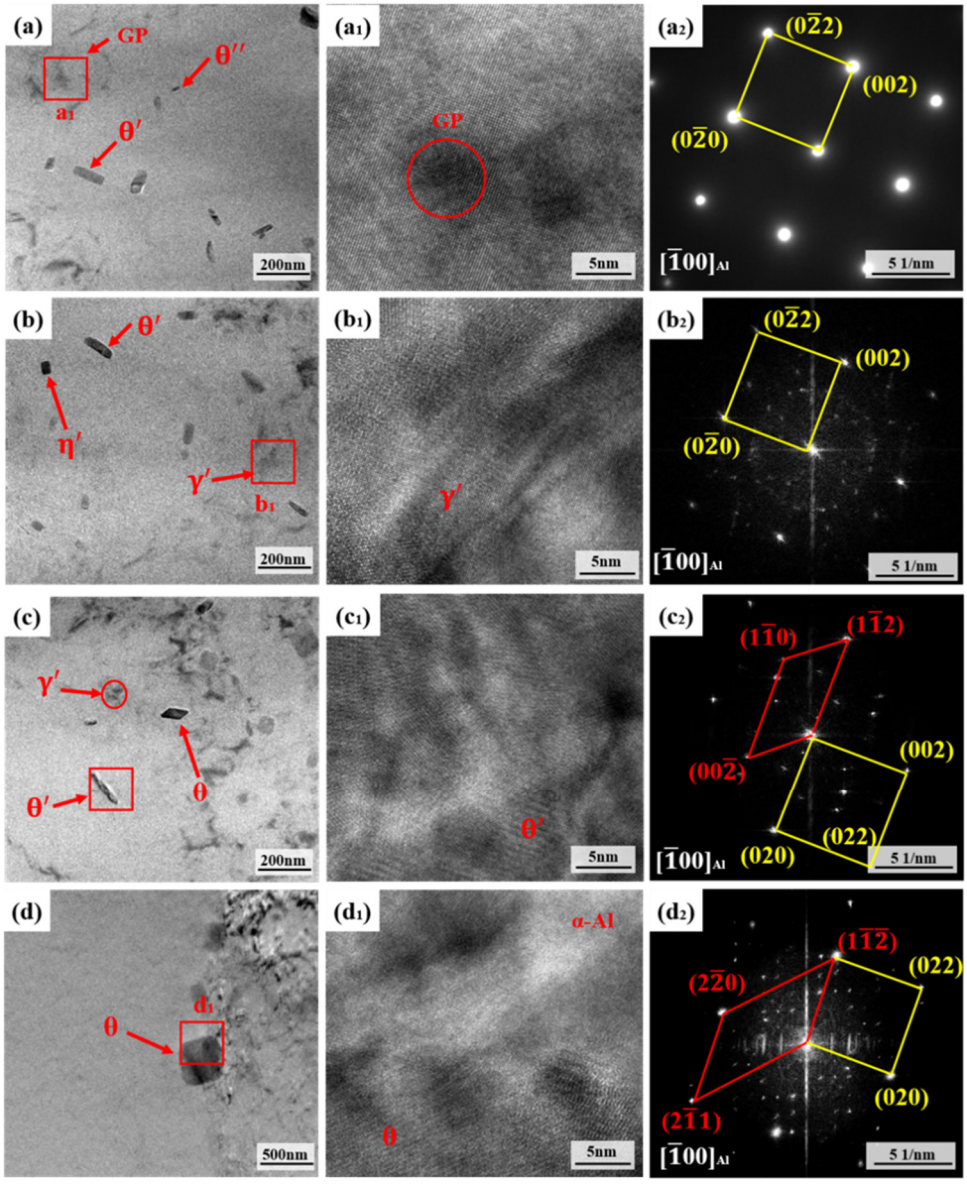

Figure 8. TEM bright field images, HRTEM images, and SAED modes of Al-Cu3-Si-Mg after aging treatment: (a) - (b) 165 °C×2 h; (c) - (d) 205 °C×6 h.

 doi:10.20944/preprints202604.1453.v1

After sufficient solution treatment, the Al-Cu3-Si-Mg alloy forms a metastable *SSS* (supersaturated solid solution). During the subsequent aging treatment, *SSS* undergoes decomposition upon holding at a certain temperature for a specific time, resulting in the formation of a series of precipitated phases. Previous study has demonstrated that several metastable transitional phases form prior to the precipitation of the equilibrium θ(Al_2Cu) phases, and the precipitation sequence is as follows [16]:

$$SSS \rightarrow \alpha_1 + GP \rightarrow \alpha_2 + \theta'' \rightarrow \alpha_3 + \theta' \rightarrow \alpha + \theta \quad (1)$$

According to the SAED analysis, GP zones are Cu-atom-enriched regions. Being coherent with the matrix, they form along the {100} plane family of α-Al, meaning Cu atoms segregate on the {100} planes of the α-Al matrix. θ''(Al_2Cu) nucleates afresh in α-Al and forms via the dissolution of GP zones. It is fully coherent with all planes of the α-Al matrix, with only slight lattice distortion along the [100] direction, appearing as disc-shaped precipitates on the habit plane. These two metastable phases are still observed in the TEM images of the Al-Cu3-Si-Mg alloy aging at 165 °C×2 h, indicating that the transformation to θ'($Al_{3.6}Cu_2$) has not been completed. In contrast, under the aging treatment of 205 °C×6 h, both metastable phases completely transform into more stable phases due to the higher temperature and longer holding time. For the solute elements Mg and Si, previous studies have indicated that the formation and subsequent transformation of their precipitated phases follow the two sequences [17,18]:

$$SSS \rightarrow \alpha_1 + GP \rightarrow \alpha_2 + \gamma' \rightarrow \alpha + \gamma \quad (2)$$

$$SSS \rightarrow \alpha 1 + GP \rightarrow \alpha 2 + \eta' \rightarrow \alpha + \eta \quad (3)$$

Under the aging treatment of 165 °C×2 h, the Al-Cu3-Si-Mg alloy undergoes the transformation of Mg-rich GP zones into γ'($Al_{0.63}Mg_{0.37}$) phases. Subsequently, after aging at 205 °C×6 h, γ'($Al_{0.63}Mg_{0.37}$) still remains in the matrix with a slight decrease in diffraction peak area, indicating that the transformation from γ'($Al_{0.63}Mg_{0.37}$) to γ(Al_3Mg_2) occurs under these two conditions but with a low fraction of transformation. In contrast, the diffraction peak area of η'(Cu_3Si) increases significantly under the condition of 205 °C×6 h, suggesting that the transformation from η'(Cu_3Si) to η(Cu_3Si) takes place at this condition with a large fraction of transformation.

Based on the above analysis and the precipitation extent of each phase under different conditions, the precipitation sequence of phases during aging treatment of the Al-Cu3-Si-Mg alloy is summarized as follows (matrix not considered): SSS → GP_0 → GP_0+γ'→GP_0+(γ'+γ)+θ''+η'→(γ'+γ)+(θ''+θ')+(η'+η)→(γ'+γ)+(θ+θ')+(η'+η)→(γ'+γ)+(θ+θ')+η→γ+θ+η. GP_0 denotes the general term for solute atom clusters in the matrix of the Al-Cu3-Si-Mg alloy.

3.2. Effect of Aging Process Parameters on Precipitates at α-Al Grain Boundaries

The precipitation behavior of θ(Al_2Cu) at grain boundaries of α-Al under different aging treatment condition is shown in Figure 9. To intuitively investigate the evolution of precipitated phases, a quantitative analysis method was employed to calculate the amounts of precipitates at grain boundaries. The length fraction f_L^θ of chain-like precipitates attached to a defined length of α-Al grain boundary was adopted, with its calculation formula given in Equation (4).

$$f_L^\theta = \frac{L_\theta}{L_\alpha} = \frac{L_1 + L_2 + \cdots + L_n}{L_\alpha} \quad (4)$$

Where L_α is the total grain boundary length of α-Al in a single field of view, $(L_1, L_2, \cdots L_n)$ are the lengths of chain-like precipitates discontinuously distributed and attached to the α-Al grain boundaries. The schematic diagram for quantitative analysis is shown in Figure 9a.

 doi:10.20944/preprints202604.1453.v1

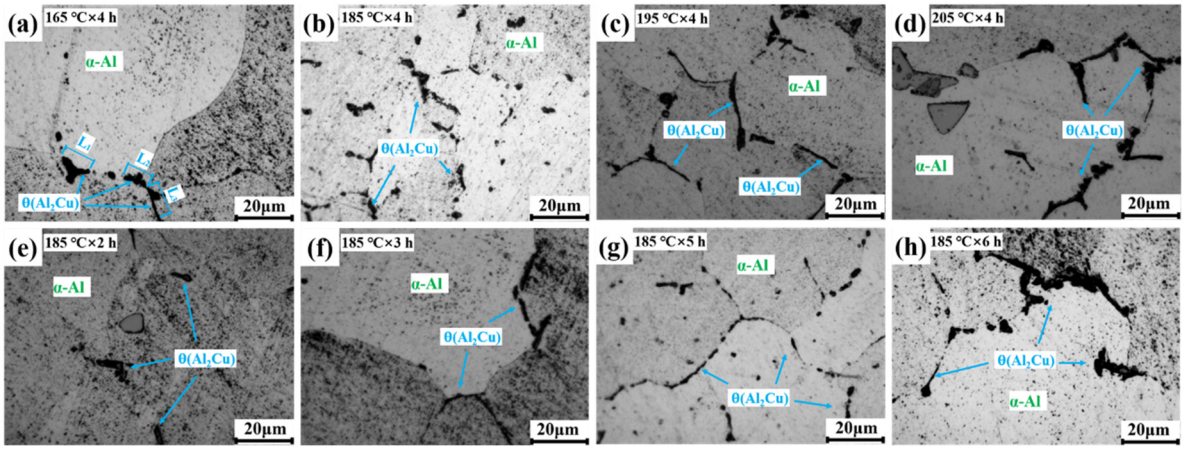

Figure 9. Precipitated phases at grain boundaries at different aging treatment condition: (a-d) different aging temperature; (e-h) different aging time.

As shown in Figure 9a, b, after aging at 165 °C and 185 °C respectively, only discontinuous chain-like θ(Al2Cu) precipitates exist at the α-Al grain boundaries, and they are mainly distributed at triple junctions. The amount of such discontinuous precipitates is relatively higher at 185 °C, with the corresponding grain boundary length fractions f_L^θ being 1.5% and 15.2%, respectively. When the aging temperature reaches 195 °C, the chain-like θ(Al2Cu) precipitates at α-Al grain boundaries exhibit a continuous distribution, as shown in Figure 9c. They appear extensively not only at triple junctions but also along the grain boundaries between two α-Al grains, with the grain boundary length fraction f_L^θ reaching 26.1%. When the aging temperature increases to 205 °C, the continuously distributed chain-like θ(Al2Cu) precipitates become even more pronounced, and the grain boundary length fraction f_L^θ reaches 43.5%. Figure 9e-h show the precipitated phases at different aging times. It can be observed that when the aging time ranges from 2 to 5 h, the θ(Al2Cu) precipitates at α-Al grain boundaries are all discontinuously distributed. With increasing aging time, the amount of these discontinuous precipitates gradually increases and tends to interconnect, with the grain boundary length fraction f_L^θ increasing from 3.2% to 32.1%. After the aging time reaches 6 h, the θ(Al2Cu) precipitates at grain boundaries show a continuous distribution, and the grain boundary length fraction f_L^θ reaches 52.6%.

The schematic diagram of the relationship between the grain boundary length fraction f_L^θ of θ(Al2Cu) in α-Al and its volume fraction f_V^θ in the α-Al matrix is shown in the Figure 10. A single equiaxed α-Al grain is assumed to be spherical with a radius of R_α. The chain-like precipitates at the grain boundaries are regarded as aggregates of S_θ spherical θ(Al2Cu) phases, distributed side by side at the grain boundaries with a width of W_θ and a length of L_θ. The radius of a single spherical θ(Al2Cu) precipitate is r_θ.

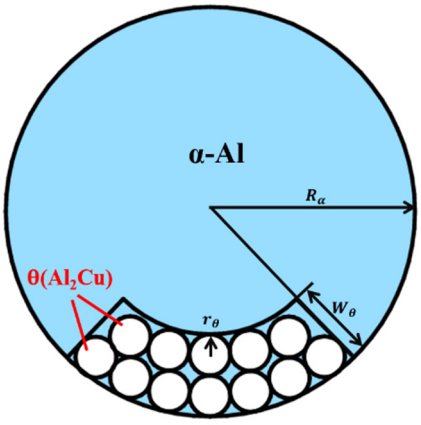

Figure 10. θ (Al2Cu) length fraction f_L^θ versus volume fraction f_V^θ diagram.

 doi:10.20944/preprints202604.1453.v1

The grain boundary length fraction of θ(Al_2Cu) in α-Al is defined as the ratio of L_θ to the perimeter of a single α-Al grain, as shown in Equation (5), where $S_{\theta L}$ represents the number of θ(Al_2Cu) precipitates along the length of the chain-like precipitates.

$$f_L^\theta = \frac{L_\theta}{2\pi R_\alpha} = \frac{S_{\theta L} r_\theta}{\pi R_\alpha} \tag{5}$$

The volume fraction f_V^θ of θ(Al_2Cu) at grain boundaries in the α-Al matrix is defined as the ratio of the total volume of spherical θ(Al_2Cu) precipitates to the volume of a single α-Al grain, as shown in Equation (6), where $S_{\theta W}$ represents the number of θ(Al_2Cu) precipitates along the width direction of the chain-like precipitates.

$$f_V^\theta = \frac{4/3\pi S_\theta r_\theta^3}{4/3\pi R_\alpha^3} = \frac{S_{\theta L} S_{\theta W} r_\theta^3}{R_\alpha^3} \tag{6}$$

From Equations (5), (6), the relationship between the length fraction f_L^θ and volume fraction f_V^θ of θ(Al_2Cu) can be obtained as shown in Equation (7).

$$f_V^\theta = \frac{\pi W_\theta r_\theta}{2R_\alpha^2} f_L^\theta \tag{7}$$

It can be seen that the volume fraction f_V^θ has a certain linear relationship with the length fraction f_L^θ. During the aging treatment, the size of α-Al matrix and θ(Al_2Cu) on the grain boundaries changes slightly, mainly reflecting the change in the quantity of precipitates. Therefore, the coefficient terms in Equations (7) can all be defined based on the size measurement. The measured average values are R_α=144μm, r_θ=0.5μm, and W_θ=2μm. The variation curves of the volume fraction f_V^θ and length fraction f_L^θ of θ(Al_2Cu) with aging time and temperature are shown in Figure 11. It can be found that the effects of aging temperature and time on the volume fraction of θ(Al_2Cu) at grain boundaries present a nonlinear relationship.

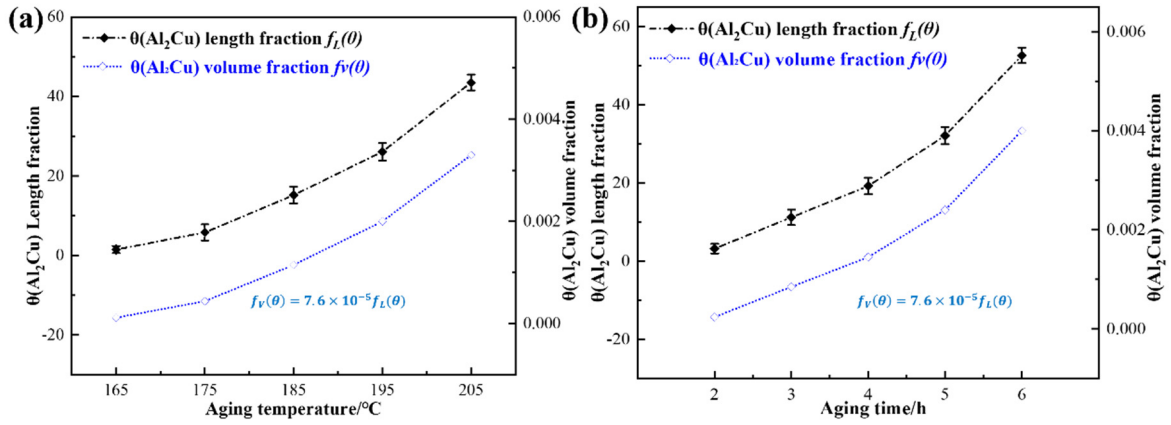

Figure 11. Variation curve of θ(Al_2Cu) precipitation fraction at grain boundary with aging parameters: (a) aging temperature; (b) aging time.

The influence of aging treatment parameters on the precipitation of θ(Al_2Cu) phase can be analyzed using the grain growth kinetics theory. It is assumed that at time t, spherical precipitate nuclei capable of growth already exist in the supersaturated α_0 matrix, and the growth regions of different precipitate particles do not overlap within a short period [19]. Suppose the initial composition of Cu in the supersaturated α_0 matrix is C_0, the matrix composition in equilibrium with the precipitate is C_α, and the composition of the θ(Al_2Cu) is C_θ, as shown in Figure 12.

 doi:10.20944/preprints202604.1453.v1

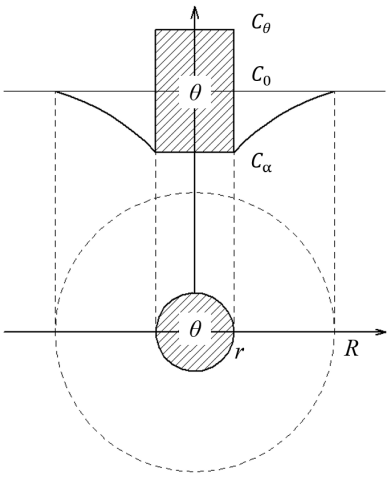

Figure 12. Schematic diagram of the growth of spherical precipitated phase.

At time t, the relationship between the average concentration $\bar{C}$ of the aluminum matrix and the precipitate fraction is shown as Equation (8).

$$z(t) = \frac{C_0 - \bar{C}}{C_0 - C_\alpha} \tag{8}$$

It is assumed that the spherical precipitates grow via diffusion, with the effects of strain energy and interfacial energy neglected. Diffusion occurs within the α_0 matrix, where solute Cu atoms diffuse toward the interface and undergo reactive diffusion at the α/θ phase boundary to form the θ(Al_2Cu) phase. During the formation of the θ(Al_2Cu), based on the quasi-steady-state diffusion approximation [20], the equation for the change in solute mass dm in the parent phase within time dt is given by Equation (9).

$$dm = \frac{4}{3}\pi R^3 d\bar{C} \tag{9}$$

According to the law of conservation of solute mass in the α and θ(Al_2Cu), the following equation is obtained:

$$\frac{4}{3}\pi r^3 C_\theta = \frac{4}{3}\pi R^3 (C_0 - \bar{C}) \tag{10}$$

Combining Equations (9), (10) and eliminating r yields Equation (11).

$$\frac{d\bar{C}}{dt} = -\frac{3D(C_0 - C_\alpha)}{R^2}\left(\frac{C_0 - \bar{C}}{C_\theta}\right)^{1/3} \tag{11}$$

Upon integration and rearrangement, the phase transformation fraction at time t is obtained as:

$$z(t) = \left[\frac{2Dt}{R^2}\left(\frac{C_0 - C_\alpha}{C_\theta}\right)^{1/3}\right]^{3/2} = \left(\frac{2t}{3\tau}\right)^{3/2} \tag{12}$$

$$\frac{1}{\tau} = \frac{3D}{R^2}\left(\frac{C_0 - C_\alpha}{C_\theta}\right)^{1/3} \tag{13}$$

It can be concluded from Equation (12) that: $z(t) \propto (t/\tau)^{3/2}$. It indicates that the precipitate fraction exhibits a nonlinear relationship with time, and increases with increasing aging time. From Equation (13), it can also be found that with increasing of aging temperature, the diffusion coefficient D increases due to the temperature dependence of diffusion, while τ decreases and $z(t)$ increases.

 doi:10.20944/preprints202604.1453.v1

This is consistent with the experimental results which both the number and size of spherical θ(Al_2Cu) phases tend to increase with increasing aging temperature and time. This result verifies the experimental results of the nonlinear curves between the volume fraction of θ(Al_2Cu) and aging temperature and time in Figure 11.

3.3. Effect of Aging Process Parameters on Precipitates within α-Al Grains

The bright-field TEM images of precipitates within α-Al grains under different aging treatment conditions are shown in Figure 13. It can be seen from Figure 13a that after aging at 165 °C×4 h, a large number of disc-shaped θ''(Al_2Cu) and θ'($Al_{3.6}Cu_2$) precipitates are formed inside the grains, with average numbers of 11 and 12, respectively. The amount of θ(Al_2Cu) is extremely low, indicating that the precipitation sequence GP → θ''(Al_2Cu) → θ'($Al_{3.6}Cu_2$) mainly occurs at this temperature, which has not reached the precipitation temperature for θ(Al_2Cu). After aging at 185 °C×4 h, it can be seen from Figure 13b that the amount of θ''(Al_2Cu) inside the grains is significantly reduced, while the quantities of θ'($Al_{3.6}Cu_2$) and θ(Al_2Cu) are obviously increased to 17 and 6 respectively, indicating that a large amount of θ''(Al_2Cu) transforms into θ' ($Al_{3.6}Cu_2$) and θ (Al_2Cu) at this temperature. As can be seen from Figure 13c, after aging at 205 °C×4 h, θ''(Al_2Cu) within the grains disappears completely, while a large number of θ (Al_2Cu) precipitates appear with a quantity of 48, and their size shows an increasing trend, indicating that at this temperature, θ''(Al_2Cu) is completely transformed into θ'($Al_{3.6}Cu_2$), and a large amount of θ'($Al_{3.6}Cu_2$) is further transformed into θ(Al_2Cu). It can also be observed from the size curve that the size of θ'($Al_{3.6}Cu_2$) decreases gradually, and the ratio of its diameter to thickness decreases with increasing temperature. This is attributed to the transformation into non-coherent spherical θ(Al_2Cu), the transformation from disc-shaped precipitates to spherical phases.

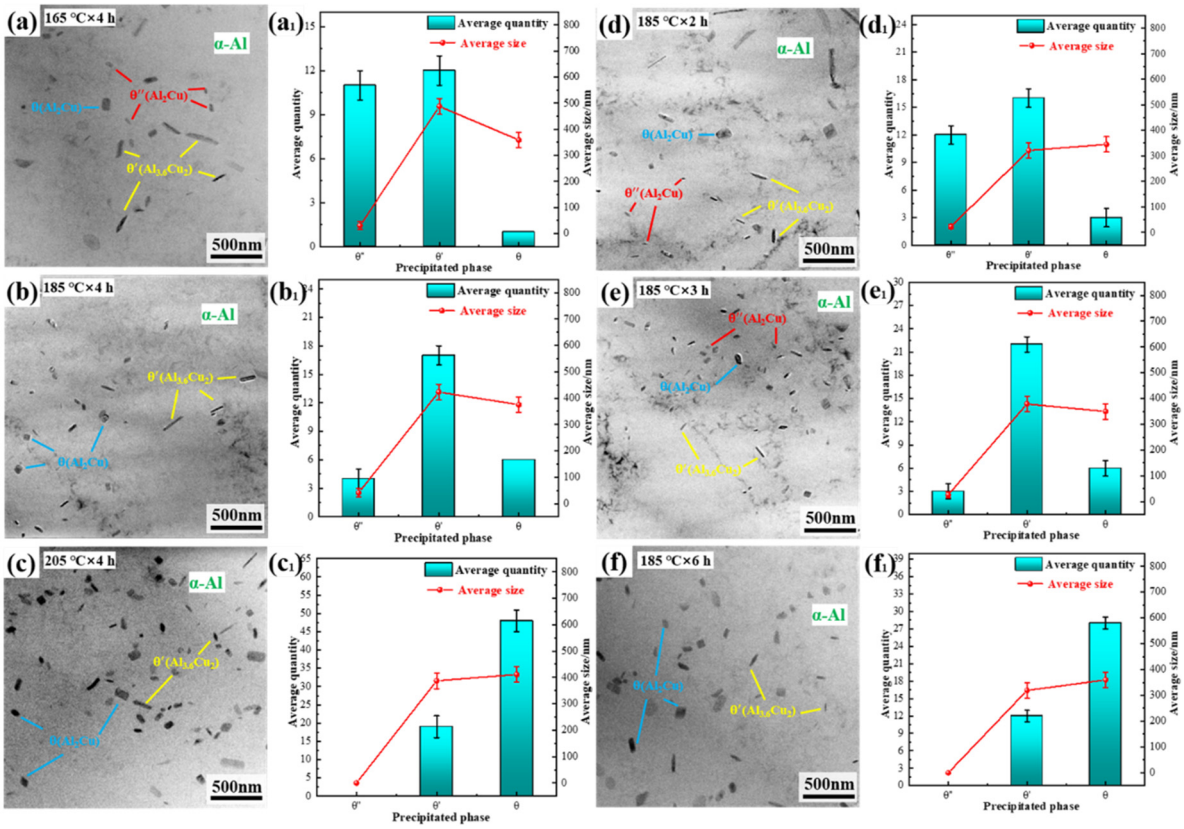

Figure 13. Bright-field TEM images of the Al-Cu3-Si-Mg alloy under different aging treatment conditions: (a-c) different aging temperature; (d-f) different aging time.

Bright-field TEM images of precipitates within α-Al grains under different aging times at aging temperature of 185 °C are shown in Figure 13d-f. It can be found that when the aging time is within

 doi:10.20944/preprints202604.1453.v1

3 h, the amount of θ(Al_2Cu) in α-Al grains is relatively small. At this stage, the precipitation reaction θ''(Al_2Cu) → θ'($Al_{3.6}Cu_2$) mainly occurs, as reflected by the drastic decrease in the amount of θ''(Al_2Cu) and the significant increase in the amount of θ'($Al_{3.6}Cu_2$), whose quantities decrease from 12 to 3 and increase from 16 to 23, respectively. After aging for 6 h, θ''(Al_2Cu) in the grains disappears completely, and the amount of θ(Al_2Cu) increases significantly to 28. Combined with Figure 13c, it can be found that under prolonged aging treatment, when the temperature increases from 185 °C to 205 °C, the quantity of θ(Al_2Cu) rises from 28 to 48, indicating that 185-205 °C is the temperature range where a large amount of θ'($Al_{3.6}Cu_2$) transforms into θ(Al_2Cu).

4. Conclusions

The evolution of precipitates during aging treatment of Al-Cu3-Si-Mg alloy prepared by MMDF was investigated. Aging treatment experiments at different temperatures and holding times were carried out, and the microstructure was characterized by XRD, OM and TEM. The precipitation mechanism and sequence of precipitates were analyzed. The main conclusions are as follows:

(1) After aging treatment, the supersaturated solid solution of the Al-Cu3-Si-Mg alloy precipitates phases dominated by θ(Al_2Cu), θ'($Al_{3.6}Cu_2$), γ'($Al_{0.63}Mg_{0.37}$) and η'(Cu, Si). Based on XRD and TEM analyses under different aging treatment conditions, the precipitation sequence of the precipitated phases is summarized as follows SSS → GP_0 → GP_0+γ' → GP_0+(γ'+γ)+θ''+η' → (γ'+γ)+(θ''+θ')+(η'+η) → (γ'+γ)+(θ+θ')+(η'+η) → (γ'+γ)+(θ+θ')+η → γ+θ+η.

(2) With increasing aging temperature and aging time, θ(Al_2Cu) precipitates aggregate at α-Al grain boundaries, forming chain-like phases. The precipitation of nanoscale phases leads to the formation of bright and dark contrasts in α-Al grains, and the number of dark-colored grains increases significantly with increasing aging temperature and time. After aging treatment of 165-185 °C×4 h, the chain-like θ(Al_2Cu) precipitates at grain boundaries are discontinuously distributed along α-Al grain boundaries. When the temperature exceeds 185 °C, the chain-like θ(Al_2Cu) precipitates at grain boundaries gradually become continuous. With increasing temperature, the length fraction f_L^θ of chain-like θ(Al_2Cu) precipitates along α-Al grain boundaries increases. Under the aging treatment of 185 °C×5-6 h, the chain-like θ(Al_2Cu) precipitates at grain boundaries gradually become more continuous, and their length fraction f_L^θ along α-Al grain boundaries continues to increase with prolonged aging time.

(3) After aging treatment of 165-185 °C×4 h, disc-shaped θ'($Al_{3.6}Cu_2$) and θ''(Al_2Cu) are mainly precipitated within the grains. When the temperature exceeds 185 °C, the amount of spherical equilibrium θ(Al_2Cu) phase in the grains increases significantly, θ''(Al_2Cu) disappears completely, and the size of θ'($Al_{3.6}Cu_2$) decreases obviously. After the aging treatment of 185 °C×5-6 h, a large number of θ'($Al_{3.6}Cu_2$) transform into θ(Al_2Cu), and their aspect ratio decreases markedly, indicating the transformation from disc-shaped to spherical morphology.

Author Contributions: Conceptualization, T. W., SM. X.; formal analysis, T. W.; investigation, T. W.; resources, T.W.; writing—original draft preparation, T. W.; writing—review and editing, T. W. and SM. X. All authors have read and agreed to the published version of the manuscript.

Data Availability Statement: Data will be made available on request.

Acknowledgments: The authors would like to express gratitude to the financial support of the MMDF research group in BeijingJiaotong University.

Conflicts of Interest: The authors declare no conflict of interest.

Abbreviations

The following abbreviations are used in this manuscript:

MMDF Molten Metal Die Forging

 doi:10.20944/preprints202604.1453.v1

References

1. Gan, Y.; Zhang, D.; Zhang, W., Li, Y. Effect of cooling rate on microstructure and mechanical properties of squeeze cast Al-Cu-Mg alloy. Int. J. Cast Met. Res. **2015**, *28*, 50-58.
2. Li, J. Y.; Lu, S. L.; Chen, L.; Liao, Q.; Guo, W.; Wu, S. S. Influence of squeeze casting pressure on nanoparticle distribution and mechanical properties of nano-SiCp/Al-Cu composites assisted with ultrasonic vibration. Trans. Nonferrous Met. Soc. China. **2023**, *33*, 1977-1987.
3. Lin, B.; Xia, S. C.; Li, H. Y.; Lou, Z. H.; Liu, K.; Zhang, W. W. Improved creep resistance of Al-Cu-Mn-Fe-Ni alloys through squeeze casting. Mater. Charact. **2019**, *158*, 109935.
4. Jiang, H.; Zhang, L. F.; Zhao, B. W.; Sun, M.; He, M. F. Microstructure and mechanical properties of ZL205A aluminum alloy produced by squeeze casting after heat treatment. Metals. **2022**, *12*, 2037.
5. Gopalakrishnan, T.; Sankaranarayanan, S. R.; Babu, S. P. K. Investigating the effect of calcium addition on the microstructural and mechanical properties of a Zn-Al-Cu-Mg alloy via squeeze casting. Metals. **2025**, *15*, 922.
6. Zhu, S.; Yang, Y.; Sui, Y. D.; Jiang, Y. H.; Wang, Q. D.; Ji, Q.; Liu, F. The effect of wall thickness on the microstructure and tensile properties on squeeze casting of Al-5Mg-2.2Si-0.6Mn-0.1Ce alloy. Int J Metalcast. **2024**, *18*, 113-122.
7. Zhang, C. X.; Liao, W. N.; Shan, Z. D.; Song, W. Z.; Dong, X. X. Squeeze casting of 4032 aluminum alloy and the synergetic enhancement of strength and ductility via Al-Ti-Nb-B grain refiner. Mater. Sci. Eng. A. **2024**, *896*, 146233.
8. Li, F.; Zhang, X. Z.; Xiong, B. J. Squeeze casting of aluminum alloy A380: Microstructure and tensile behavior. China Foundry. **2015**, *12*, 367-374.
9. Lee, H.; Bang, J.; Yoon, P.; Lee, E. Effects of combined Cr, Mn, and Zr additions on the microstructure and mechanical properties of Al-6Cu alloys under various heat treatment conditions. Metals. **2026**, *16*, 143.
10. Dar, M. S.; Liao, H. C.; Xu, A. Q. Effect of Cu and Mn content on solidification microstructure, T-phase formation and mechanical property of Al-Cu-Mn alloys. J. Alloys Compd. **2018**, *774*, 758-767.
11. Gazizov, M.; Marioara, D. C.; Friis, J.; Wenner, S.; Holmestad, R.; Kaibyshev, R. Precipitation behavior in an Al-Cu-Mg-Si alloy during ageing. Mater. Sci. Eng. A. **2019**, *767*, 138369.
12. Kim, K.; Roy, A.; Gururajan, M. P.; Wolverton, C.; Voorhees, P. W. First-principles/Phase-field modeling of θ' precipitation in Al-Cu alloys. Acta Mater. **2017**, *140*, 344-354.
13. Tohid, N.; Daniel, L.; Pierre, H.; Remi, M.; Francis, B.; Denis, M. Multiphase modelling of the growth kinetics of precipitates in Al-Cu alloys during artificial aging. Philos. Mag. **2021**, *101*, 1-24.
14. Wu, T.; Xing, S. M.; Liu, X. Study on non-equilibrium solidification microstructure of Al-Cu3-Si-Mg alloy by MMDF, Mater. Res. Express. **2022**, *9*, 046509.
15. Maksimovic, V.; Tolley, A.; Jovanovic, M. T.; Radmilovic, V. Aging of a commercial Al-Cu-Si based alloy modified with germanium. Mater. Sci. Forum. **2004**, *490*, 323-328.
16. Shin, D.; Shyam, A.; Lee, S.; Yamamoto, Y.; Haynes, J. Solute segregation at the Al/θ′-Al2Cu interface in Al-Cu alloys. Acta Mater. **2017**, *141*, 327-340.
17. Jia, Z. H.; Ding, L. P.; Cao, L. F.; Sanders, R.; Li, S. C.; Liu, Q. The influence of composition on the clustering and precipitation behavior of Al-Mg-Si-Cu alloys. Metall. Mater. Trans. **2017**, *48*, 459-473.
18. Elsebaie, O.; Samuel, M. A.; Samuel, F. H.; Doty, H.W. Impact toughness of Al-Si-Cu-Mg-Fe cast alloys: Effects of minor additives and aging conditions. Mater. Des. **2014**, *60*, 496-509.
19. Zhang, M. S.; Liu, K. L.; Wang, B. Liang, T. T.; Han, J. Q.; Wang, J. S. Accelerating pore nucleation and eutectic Si growth kinetics by increasing Cu and Sc for Al-Si-Mg alloys: In-situ observation. J. Alloys Compd. **2021**, *869*, 159173.
20. Wang, X. Y.; Hou, J. P.; Gong, B. S.; Qu, Z.; Liu, H. Z.; Wang, Q.; Zhang, Z. J.; Zhang, Z. F. Simultaneously improving strength and plasticity of Al-Cu alloy by introducing spherical precipitates. Adv. Eng. Mater. **2023**, *26*, 2301575.